zoonotic diseases

MDPI

Article

Molecular Dynamics and Optimization Studies of Horse Prion Protein Wild Type and Its S167D Mutant

Jiapu Zhang

Centre for Smart Analytics, Institute of Innovation, Science and Sustainability (IISS), The Federation University Australia, Ballarat, VIC 3350, Australia; j.zhang@federation.edu.au

Simple Summary: Prion diseases, also called transmissible spongiform encephalopathies (TSEs), are fatal neurodegenerative diseases. Prion disease has not been reported in horses up to now; therefore, horses are known to be a species resistant to prion diseases. Residue S167 in horses has been cited as a critical protective residue for encoding PrP conformational stability in prion-resistance. This article focuses on molecular dynamics and optimization studies on the horse PrP wild type and its S167D mutant, respectively, to understand their conformational dynamics and optimized conformation.

Abstract: Prion diseases, also called transmissible spongiform encephalopathies (TSEs), are fatal neurodegenerative diseases characterised by the accumulation of an abnormal prion protein isoform (PrP^{Sc}: rich in β-sheets—about 30% α-helix and 43% β-sheet), which is converted from the normal prion protein (PrP^{C}: predominantly α-helical—about 42% α-helix and 3% β-sheet). However, prion disease has not been reported in horses up to now; therefore, horses are known to be a species resistant to prion diseases. Residue S167 in horses has been cited as a critical protective residue for encoding PrP conformational stability in prion-resistance. According to the "protein-only" hypothesis, PrP^{Sc} is responsible for both the spongiform degeneration of the brain and disease transmissibility. Thus, understanding the conformational dynamics of PrP^{Sc} from PrP^{C} is key to developing effective therapies. This article focuses on molecular dynamics and optimization studies on the horse PrP wild type and its S167D mutant, respectively, to understand their conformational dynamics and optimized confirmation; the interesting results will be discussed.

Keywords: horse prion protein; protective residue S167; S167D mutant; molecular dynamics and optimization studies; secrets of resisting prion diseases

Citation: Zhang, J. Molecular Dynamics and Optimization Studies of Horse Prion Protein Wild Type and Its S167D Mutant. *Zoonotic Dis.* **2024**, *4*, 187–200. https://doi.org/10.3390/zoonoticdis4030017

Academic Editor: Stephen K. Wikel

Received: 19 May 2024
Revised: 20 July 2024
Accepted: 29 July 2024
Published: 1 August 2024

1. Introduction

Prion diseases are incurable neurodegenerative diseases caused by aberrant conformations of the prion protein (PrP). Many animals develop similar diseases, but rabbits, dogs, and horses show unusual resistance to prion diseases [1–15]. This resistance could be due to protective changes in the sequence of the corresponding PrP in each animal. Structural studies have identified S174, S167 and D159 as the key protective residues in rabbit, horse and dog PrP, respectively [1–15]. But no systemic molecular dynamics (MD) studies currently support the protective activity of these residues, especially for the horse PrP residue S167. Experimental laboratory results revealed that expression of horse PrP-S167D (which carries a substitution for the equivalent residue in the PrP of hamsters, a species that is susceptible to prion diseases) shows high toxicity in behavioural and anatomical assays [14]. Thus, this article aims to carry out an MD study of the horse PrP wild-type (WT) NMR structure 2KU4.pdb and an optimization study of the S167D mutant (hereafter, mutant) homology structure (constructed by this article). We will present in this article useful protective bioinformatics of S167 and discuss the structural features that make horse PrP more stable. The findings of this article might contribute to the development

of drugs/compounds that stabilize the PrP structure and prevent the formation of toxic conformations of prion diseases.

Here, we detail the central topic on PrP more in this introduction section. Unlike bacteria and viruses which are based on DNA and RNA, prions are unique as disease-causing agents since they are misfolded proteins. Prion contains no nucleic acids, and it is a misshapen or conformationally changed protein that acts like an infectious agent. Prion diseases are called "protein structural conformational" diseases. Normal prion protein is denoted as PrP^{C} and diseased infectious prion is denoted as PrP^{Sc}. PrP^{C} is predominant in α-helices, but PrP^{Sc} is rich in β-sheets in the form of amyloid fibrils. PrP^{C} is a normal protein found on the membranes of cell, including several blood components of which platelets constitute the largest reservoir in humans. Several topological forms exist; one cell-surface form anchored via glycolipid and two transmembrane forms. The normal protein has a complex function, which continues to be investigated at present; the cleavage of PrP^{C} in peripheral nerves causes the activation of myelin repair in Schwann cells, PrP^{C} regulates cell death, PrP^{C} may have a function in the maintenance of long-term memory, PrP^{C} may play roles in innate immunity and stem cell renewal, etc. PrP^{C} binds Cu^{2+} ions with high affinity; the significance of this property is not clear, but it is presumed to relate to the protein's structure or function. PrP^{C} is not sedimentable, meaning it cannot be separated by centrifuging techniques. PrP^{C} is readily digested by proteinase K and can be liberated from the cell surface by the enzyme phosphainositide phospholipase C, which cleaves the glycophosphatidylinositol glycoplipid anchor. PrP^{C} plays an important role in cell–cell adhesion and intracellular signaling in vivo and may therefore be involved in cell–cell communication in the brain. PrP^{Sc} always causes prion disease. Several highly infectious, brain-derived PrP^{Sc} structures have been discovered by cryo-EM; another brain-derived fibril structure isolated from humans with the prion disease GSS syndrome has also been determined. Often, PrP^{Sc} is bound to cellular membranes, presumably via its array of glycolipid anchors; however, sometimes the fibres are dissociated from membranes and accumulate outside of cells in the form of plaques. S167 in PrP^{C} is a protective residue and generates a more compact and stable structure in the C-terminal subdomain of the PrP^{C} global domain [15,16].

2. Materials and Methods

The material is the same as that of [13]: the NMR structure 2KU4.pdb of horse PrP WT (119–231). Based on 2KU4.pdb, we make only one mutation, S167D, at position 167 from the hamster PrP residue ASP167 and obtain a homology structure for an S167D mutant of horse PrP. The optimization-study methods for the S167D mutant are referred from [17], i.e., taking into account the three-body movement we use the hybrid local search optimization method.

For both the WT and the mutant, the low pH in the MD simulations is achieved by the change of the residues HIS, ASP and GLU into HIP, ASH and GLH, respectively, and the Cl- ions added by the XLEaP module of the AMBER package, and the neutral pH in the MD simulations is achieved by the change of the residues HIS into HID and the Na^{+} ions added by the XLEaP module of the AMBER package.

The MD simulations are performed at 300 K, 350 K and 450 K, respectively, as Section 1.2 of [18] described; in order to make our description convenient for readers and for reproducibility, we list these as (I)–(III) as follows. (I) At 300 K: MD simulations used the ff03 force field of the AMBER package (ambermd.org), in neutral or low-pH environments (where the residues HIS were changed into HID by the XLEaP module of the AMBER package in order to obtain a neutral pH environment). The systems were surrounded with a 12 Å layer of TIP3PBOX water molecules and neutralized by sodium (Na^{+} or Cl^{-}) ions using the XLEaP module of the AMBER package. The solvated proteins with their counter-ions were minimized mainly by the steepest descent method and then a small number of conjugate gradient steps were performed on the data, in order to remove bad hydrogen bond (HB), etc., contacts. Then, the solvated proteins were heated from 100 to

300 K during 300 ps and then kept at 300 K for 700 ps, both in the constant NVT ensemble using Langevin thermostat algorithm. The SHAKE algorithm and PMEMD algorithm with nonbonded cut-offs of 12 Å were used during the heating. Enough equilibrations had been performed in the constant NPT ensemble under a Berendsen thermostat during 5 ns until the RMSD, press, volume and density were sufficiently stable, where the RMSD values did not fluctuate very much within a few picoseconds. After equilibrations, a production MD phase was carried out at 300 K for 30 ns using a constant pressure and temperature NPT ensemble and the PMEMD algorithm with nonbonded cutoffs of 12 Å during the production simulations. The step size for equilibration is 0.5 fs, and 1 fs for the production runs. The structures were saved to file every 1000 steps. The MD for each structure was finished in 36 ns. (II) At 350 K: 350 K might be a practical temperature for many experimental laboratory works. MD simulations used the ff03 force field of the AMBER package, in neutral and low-pH environments (where the residues HIS, ASP and GLU were changed into HIP, ASH and GLH, respectively, by the XLEaP module of the AMBER package in order to obtain the low-pH environment). The systems were surrounded with a 12 Å layer of TIP3PBOX water molecules and neutralized by sodium ions using the XLEaP module of the AMBER package. The solvated proteins with their counterions were minimized mainly by the steepest descent method and then a small number of conjugate gradient steps were performed on the data, in order to remove bad contacts. Then, the solvated proteins were heated from 100 to 300 K during 1 ns (with step size 1 fs) and from 300 to 350 K during 1 ns (with step size 2 fs). The thermostat algorithm used is the Langevin thermostat algorithm in constant NVT ensembles. The SHAKE algorithm and PMEMD algorithm with nonbonded cutoffs of 12 Å were used during the 2 ns heating. Equilibrations were performed in constant NPT ensembles under a Langevin thermostat for 2 ns. After equilibrations, the production MD phase was carried out at 350 K for 30 ns using a constant pressure and temperature NPT ensemble and the PMEMD algorithm with nonbonded cutoffs of 12 Å during simulations. The step size for the production runs is 2 fs. The structures were saved to file every 1000 steps. The MD was finished for each structure in 34 ns. (III) At 450K*:* The MD simulations used the ff03 force field of the AMBER package, in neutral and low-pH environments. The systems were surrounded with a 12 Å layer of TIP3PBOX water molecules and neutralized by sodium ions using the XLEaP module of the AMBER package. The solvated proteins with their counterions were minimized mainly by the steepest descent method and then a small number of conjugate gradient steps were performed on the data, in order to remove bad contacts. Then, the solvated proteins were heated from 100 to 450 K step by step during 3 ns. The thermostat algorithm used is the Langevin thermostat algorithm in constant NVT ensembles. The SHAKE algorithm and PMEMD algorithm with nonbonded cutoffs of 12 Å were used during the heating. Equilibrations were performed in constant NPT ensembles under a Langevin thermostat for 5 ns. After equilibrations, the production MD phase was carried out at 450 K for 30 ns using a constant pressure and temperature NPT ensemble and the PMEMD algorithm with nonbonded cutoffs of 12 Å during production simulations. The step size for equilibration was 0.5 fs, and 1 fs for the production runs. The structures were saved to file every 1000 steps. The MD was finished in each structure in 38 ns.

The study utilized a computational approach to study the conformational stability of the target protein. For the mutant, the decision to use homology modelling rather than in silico mutagenesis was made because currently the experimental structure of the S167D mutant is not produced by an NMR/X-ray/cryo-EM lab yet; the rationale behind selecting this method is high—the author's experiences show us that for a molecular structure, making only one mutation usually provides much better agreement with the experimental laboratory NMR/X-ray/cryo-EM structure. However, for a molecular structure, if at the same time two mutations are made, the homology structure is usually so far from the laboratory structure that it is not reliable to use the homology structure. This is a point we should highlight in the real applications of this study.

We should also note that in this article three dynamic replicas were performed, and the results are not the average of the dynamics.

3. Results and Discussion

For convenience, we give some acronyms. For the WT horse normal cellular prion protein [12] (horse PrP^C with PDB entry 2KU4), its structural region GLY119-SER231 consists of β-strand 1 (β1: MET129-ALA133), α-helix 1 (α1: ASP144-ARG151), 3_{10}-helix 1 (3_{10}H1: MET154-ARG156), β-strand 2 (β2: GLN160-TYR163), 3_{10}-helix 2 (3_{10}H2: VAL166-GLU168), α-helix 2 (α2: GLN172-THR192), α-helix 3 (α3: GLU200-ARG228) and the loops linking them each other. As we all know, the stability of a protein is maintained by its salt bridges, hydrogen bonds, hydrophobic contacts, van der Waals contacts and disulfide bonds (for the PrP monomer there exists a disulfide bond (S-S) between CYS179 and CYS214), etc., to drive the ability to perform the biological function of the protein; we denote SBs, HBs, HYDs, vdWs for salt bridges, hydrogen bonds, hydrophobic interactions and van der Waals contacts, respectively. We denote amino acids (or residues) as 'aa.' Residue 167 is in the β2-α2 loop of PrPs, and both Syrian hamsters and horses have a well-defined and highly ordered β2-α2 loop.

Firstly, we optimized the WT and mutant structures, and their backbone atoms' RMSD (root mean square deviation) value is 0.495090 angstroms (Figure 1). We found the mutation had the following consequences: (i) for the secondary structures in the segment TYR169-ASN171 (before the N-terminal of α2), the turn is changed into a coil; in the segment LYS194-GLU196 (next to the C-terminal of α2) the coil is changed into a turn and extends the C-terminal α1 from the bend–turn structure in the segment GLU152-ASN153; (ii) for the SBs, ASP147-ARG148 (in α1), ASP147-ARG151 (in α1), ASP178-HIS177 (in α2), ASP202-ARG156 (linking α3-3_{10}H1), GLU152-ARG151 (linking α1-3_{10}H1-loop-α1), GLU168-ARG164 (linking 3_{10}H2-β2-3_{10}H2-loop), GLU200-LYS204 (in α3), GLU211-ARG208 (in α3) and GLU221-LYS220 (in α3) (except for ASP144-ARG148 (in α1), GLU196-ARG156 (linking α2-α3-loop-3_{10}H1)) disappeared in the mutant; (iii) for the HBs, there are 12 HBs less than in WT (see details in Table 1—we illuminate the importance of the HB ASH/ASP202.OD1-TYR149.OH of the WT in Figure 2, though it is weak during the 30 ns MDs but not existing in the optimized structure of the mutant); and (iv) for the π-interactions, the π-cations PHE141-ARG208.$NH2^+$ (linking β1-α1-loop-α3) and HIS177-LYS173.NZ^+ (in α2) disappeared in the mutant. Residue 167 is in the β2-α2-loop and the mutation S167D results in increased negative charges on the surface around the β2-α2-loop region (ASP is a negatively charged residue) (Figure 3).

Table 1. The S167D mutation made changes in the network of hydrogen bonds (HBs).

HBs Kept	Locations	HBs Lost	Locations
ARG228.N-ALA224.O	in α3	TYR149.OH-ASP202.OD1	α1–α3
ASN181.N-HIS177.O	in α2	ASN153.ND2-TYR149.O	α1-3_{10}H1-loop-α1
CYS179.N-PHE175.O	in α2	ARG156.N-ASN153.O	3_{10}H1-α1-3_{10}H1-loop
CYS214.N-VAL210.O	in α3	ARG164.NE-GLU168.OE2	β2-3_{10}H2-loop-3_{10}H2
GLN217.N-MET213.O	in α3	ARG164.NH2-GLU168.OE1	β2-3_{10}H2-loop-3_{10}H2
GLU207.N-VAL203.O	in α3	HIS177.ND1-ASP178.OD1	in α2
GLU211.N-GLU207.O	in α3	ASP178.N-ASN174.O	in α2
GLU221.N-GLN217.O	in α3	HIS187.N-THR183.O	in α2
GLY131.N-VAL161.O	β1–β2	THR192.N-THR188.O	in α2
HIS177.N-LYS173.O	in α2	LYS194.N-THR191.O	α2-α3-loop-α2
ILE182.N-ASP178.O	in α2	GLU196.N-THR191.OG1	α2-α3-loop-α2
ILE205.N-THR201.O	in α3	PHE198.N-THR192.OG1	α2-α3-loop-α2

Table 1. *Cont.*

HBs Kept	Locations	HBs Lost	Locations
ILE215.N-GLU211.O	in α3	GLN212.NE2-GLU211.OE2	in α3
LYS185.N-ASN181.O	in α2	GLN217.NE2-TYR163.OH	α3-β2
LYS204.N-GLU200.O	in α3	GLN219.NE2-ILE215.O	in α3
MET129.N-TYR163.O	β1–β2	GLN227.NE2-GLU223.O	in α3
MET134.N-ASN159.O	β1-α1-loop-3_{10}H1-β2-loop	SER231.OG-GLN227.O	C-terminal-α3
MET206.N-ASP202.O	in α3		
MET213.N-VAL209.O	in α3	new HBs	locations
PHE225.N-GLU221.O	in α3	TYR150.N-GLU146.O	in α1
THR183.OG1-CYS179.O	in α2	ARG151.N-ASP147.O	in α1
THR188.N-VAL184.O	in α2	GLU152.N-ARG148.O	α1-3_{10}H1-loop-α1
THR190.N-GLN186.O	in α2	ASN171.ND2-ASN174.OD1	3_{10}H2-α2-loop-α2
THR216.N-GLN212.O	in α3	GLN186.N-ILE182.O	in α2
TYR149.N-TYR145.O	in α1		
TYR150.OH-PRO137.O	α1-β1-α1-loop		
TYR162.N-THR183.OG1	β2-α2		
TYR218.N-CYS214.O	in α3		
TYR222.N-TYR218.O	in α3		
VAL176.N-GLN172.O	in α2		
VAL180.N-VAL176.O	in α2		
VAL184.N-VAL180.O	in α2		
VAL189.N-LYS185.O	in α2		
VAL203.N-THR199.O	α3-α2-α3-loop		
VAL209.N-ILE205.O	in α3		
VAL210.N-MET206.O	in α3		

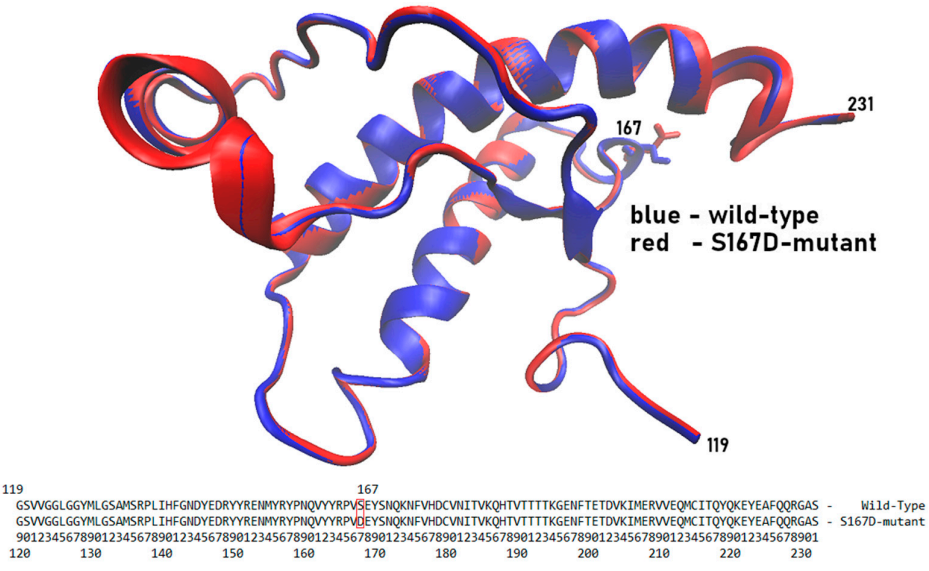

Figure 1. Performing a three-dimensional structural alignment (with an RMSD value of 0.495090 Å) and a primary sequence alignment of the horse PrP wild type and its S167D mutant. In the red box, they are the residues that differ from the wild-type to the mutant each other at position 167.

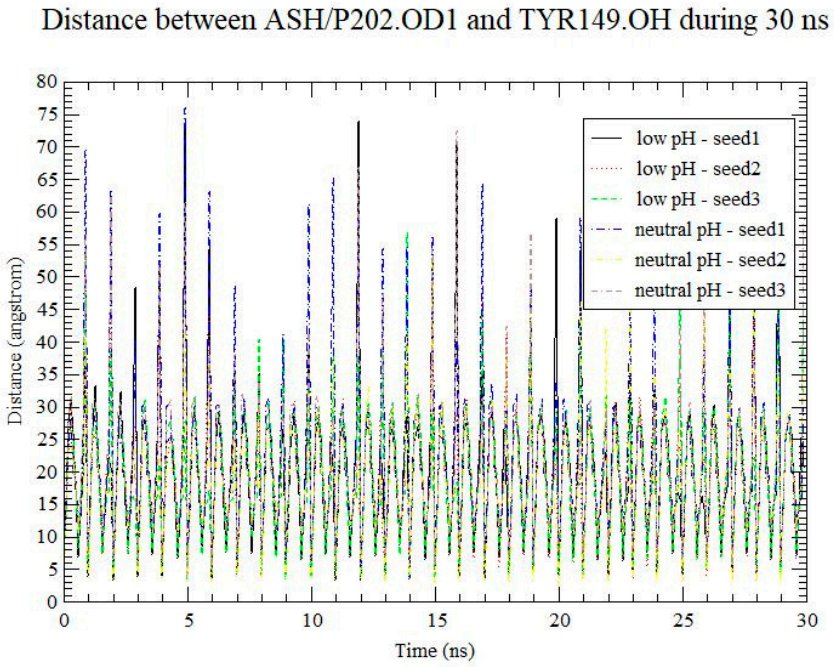

Figure 2. The importance of HB ASH/ASP202.OD1-TYR149.OH of the WT. It is weak during the 30 ns MDs but it does not exist in the optimized structure of the S167D mutant.

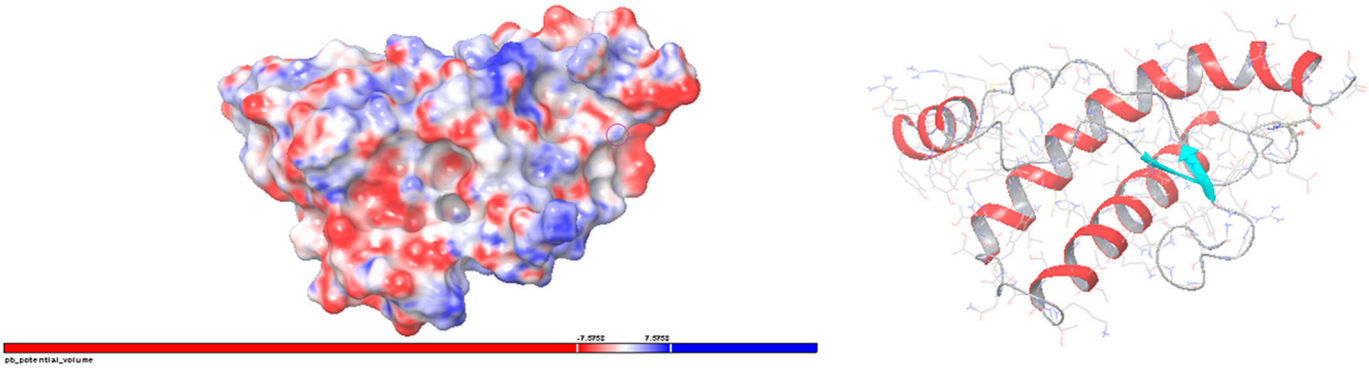

Figure 3. Residue 167 is in the β2-α2-loop and the mutation S167D results in increased negative charges on the surface around the β2-α2-loop region (ASP is a negatively charged residue—blue-coloured and circled in the Poisson–Boltzmann electrostatic potential surface); the right graph is the three-dimensional structure of the S167D mutant.

Because the S167D mutation resulted in some lost HBs and SBs in α2 and α3 and some lost π-cations, we may see that the molecular structure of the mutant (compared with the WT) is unstable especially in the regions of α2 and α3 (especially at both terminals of α2). On the contrary, in Section 4.1 of [18], the MD results show that the N-terminal half of α1 is not stable at 350 K and 450 K, but the β2-α2-loop has less variation than other PrP loops due to being the well-defined and highly ordered β2-α2-loop structure of horse PrP. These results imply to us that the S167D mutation reversed the MD results of [18]—S167 is critical to the contribution of horse PrP^C structure stability.

The above is just a snapshot of the results of the WT or mutant. Next, let us study the 30 ns MD results of the WT.

We first consider the secondary structure developments (Table 2 and Figures S1–S3), HBs (Table 3), SBs (Table 4) and HYDs (Tables 5 and 6) results of 30 ns MDs of the WT.

Table 2. Secondary Structures percentages of the WT at 300K, 350 K and 450 K during 30 ns MD simulations (seed1, seed2, seed3) in neutral and low-pH environments.

			B β-Bridge	G 3_{10}-Helix	I π-Helix	H α-Helix	E β-Sheet	T Turn	S Bend
300 K	Low pH	Seed1	0.00%	4.88%	0.00%	50.41%	3.54%	7.79%	7.65%
		Seed2	0.26%	3.32%	0.09%	48.54%	4.63%	8.34%	9.00%
		Seed3	0.21%	4.44%	0.00%	46.63%	4.07%	8.93%	10.89%
	Neutral pH	Seed1	0.00%	4.53%	0.00%	51.20%	3.54%	5.04%	8.73%
		Seed2	0.13%	3.94%	0.03%	50.15%	3.55%	9.00%	7.94%
		Seed3	0.50%	2.90%	0.00%	51.17%	3.73%	8.34%	8.83%
350 K	Low pH	Seed1	0.21%	2.85%	0.00%	49.39%	3.42%	8.34%	10.18%
		Seed2	0.34%	3.55%	0.03%	48.73%	4.11%	9.05%	9.11%
		Seed3	0.37%	3.24%	0.00%	49.29%	4.14%	8.67%	8.20%
	Neutral pH	Seed1	0.47%	4.90%	0.00%	46.79%	4.96%	9.62%	7.92%
		Seed2	0.18%	3.60%	0.03%	49.18%	3.49%	9.04%	9.60%
		Seed3	0.67%	4.70%	0.03%	49.53%	4.31%	6.76%	9.19%
450 K	Low pH	Seed1	1.09%	3.47%	0.09%	42.18%	1.17%	12.46%	12.70%
		Seed2	0.93%	4.85%	0.12%	41.37%	3.60%	14.31%	12.84%
		Seed3	0.76%	4.25%	0.06%	38.34%	3.14%	14.80%	15.43%
	Neutral pH	Seed1	0.81%	4.35%	0.00%	38.38%	0.64%	16.43%	14.61%
		Seed2	0.73%	4.09%	0.12%	42.47%	3.33%	11.43%	14.64%
		Seed3	0.28%	4.07%	0.09%	45.13%	4.05%	10.64%	7.31%

Table 3. All HBs (with % occupied rates > 10% for seed1, seed2 and seed3) of the WT at 300 K, 350 K and 450 K under a neutral pH environment during the whole 3 sets of 30 ns MD simulations for each temperature level.

HBs at 300 K under Neutral pH Environment	HBs at 350 K under Neutral pH Environment	HBs at 450 K under Neutral pH Environment
ASP202@OD1-TYR157@OH.HH 29.19, 84.64, 44.75	GLU196@O-ARG$^+$156@NE.HE 10.27, 12.50, 0	ASP202@OD1-ARG$^+$156@NE.HE 0, 0, 11.57
ASP202@OD2-TYR157@OH.HH 62.79, 0, 49.53	GLU196@O-ARG$^+$156@NH1.HH12 0, 0, 17.27	ASP202@OD1-ARG$^+$156@NH1.HH12 23.27, 28.72, 14.80
ASP202@OD1-ARG$^+$156@NH1.HH11 0, 67.38, 0	GLU196@O-ARG$^+$156@NH2.HH21 21.24, 0, 0	ASP202@OD1-ARG$^+$156@NH2.HH21 0, 5.00, 14.12
ASP202@OD1-ARG$^+$156@NH1.HH12 60.02, 0, 42.64	GLU196@O-ARG$^+$156@NH2.HH22 0, 0, 12.43	ASP202@OD1-ARG$^+$156@NH2.HH22 16.40, 20.87, 16.53
ASP202@OD2-ARG$^+$156@NH1.HH12 28.89, 0, 42.91	GLU196@OE1-ARG$^+$156@NH2.HH21 0, 17.91, 0	ASP202@OD2-ARG$^+$156@NE.HE 0, 0, 10.60
ASP202@OD1-ARG$^+$156@NH2.HH22 33.65, 0, 48.65	GLU196@OE2-ARG$^+$156@NE.HE 0, 10.62, 13.05	ASP202@OD2-ARG$^+$156@NH1.HH12 17.80, 22.15, 17.12
ASP202@OD2-ARG$^+$156@NH2.HH22 60.77, 0, 43.96	GLU196@OE2-ARG$^+$156@NH2.HH21 0, 0, 11.42	ASP202@OD2-ARG$^+$156@NH2.HH21 0, 0, 15.88
ASP202@OD1-TYR149@OH.HH 0, 12.02, 0	ASP202@OD1-TYR149@OH.HH 0, 19.46, 18.03	ASP202@OD2-ARG$^+$156@NH2.HH22 21.58, 27.68, 13.57
ASP202@OD2-TYR149@OH.HH 0, 67.42, 0	ASP202@OD2-TYR149@OH.HH 0, 22.37, 41.93	ASP202@OD1-TYR157@OH.HH 0, 20.78, 32.18
ASP178@OD2-TYR128@OH.HH 27.04, 0, 0	ASP202@OD1-ARG$^+$156@NE.HE 0, 0, 10.28	ASP202@OD2-TYR157@OH.HH 0, 22.68, 29.00
ASP178@OD1-TYR128@OH.HH 25.90, 0, 12.08	ASP202@OD1-ARG$^+$156@NH1.HH11 0, 0, 45.58	ASP202@OD1-TYR149@OH.HH 0, 7.25, 10.40
ASP178@OD2-ARG$^+$164@NH2.HH21 0, 82.87, 40.21	ASP202@OD1-ARG$^+$156@NH1.HH12 49.23, 24.93, 0	GLU196@OE1-GLY119@N.H1 10.47, 0, 0
ASP178@OD1-ARG$^+$164@NE.HE 0, 61.45, 30.03	ASP202@OD1-ARG$^+$156@NH2.HH21 0, 0, 10.11	GLU196@OE1-SER120@OG.HG 12.35, 0, 0
ASP178@OD1-ARG$^+$164@NH2.HH21 0, 22.19, 30.73	ASP202@OD1-ARG$^+$156@NH2.HH22 31.87, 28.07, 0	ASP178@OD1-ARG$^+$164@NE.HE 0, 11.82, 8.88
ASP178@OD2-ARG$^+$164@NE.HE 0, 0, 13.35	ASP202@OD2-ARG$^+$156@NH1.HH11 0, 20.97, 0	ASP178@OD1-ARG$^+$164@NH1.HH11 0, 0, 18.53
GLU146@OE1-LYS$^+$204@NZ.HZ1 0, 16.53, 0	ASP202@OD2-ARG$^+$156@NH1.HH12 28.89, 26.21, 0	ASP178@OD1-ARG$^+$164@NH1.HH12 11.90, 0, 0
GLU146@OE2-LYS$^+$204@NZ.HZ1 0, 16.10, 0	ASP202@OD2-ARG$^+$156@NH2.HH21 0, 0, 14.52	ASP178@OD1-ARG$^+$164@NH2.HH21 0, 17.60, 12.73

Table 3. *Cont.*

HBs at 300 K under Neutral pH Environment	HBs at 350 K under Neutral pH Environment	HBs at 450 K under Neutral pH Environment
GLU146@OE2-LYS$^+$204@NZ.HZ2 0, 16.09, 0	ASP202@OD2-ARG$^+$156@NH2.HH22 45.29, 18.65, 0	ASP178@OD2-ARG$^+$164@NH1.HH11 0, 0, 16.20
GLU146@OE1-LYS$^+$204@NZ.HZ2 0, 15.53, 0	ASP202@OD1-TYR157@OH.HH 43.71, 27.18, 66.71	ASP178@OD2-ARG$^+$164@NH1.HH12 10.07, 0, 0
GLU146@OE1-LYS$^+$204@NZ.HZ3 0, 17.57, 0	ASP202@OD2-TYR157@OH.HH 30.47, 57.38, 0	ASP178@OD2-ARG$^+$164@NH2.HH21 7.88, 18.63, 13.17
GLU146@OE2-LYS$^+$204@NZ.HZ3 0, 17.39, 0	ASP178@OD1-ARG$^+$164@NE.HE 13.48, 23.84, 15.06	ASP178@OD1-TYR169@OH.HH 0, 27.60, 15.75
GLN172@OE1-GLN219@NE2.HE21 10.89, 0, 0	ASP178@OD1-ARG$^+$164@NH2.HH21 24.08, 15.08, 23.03	ASP178@OD2-TYR169@OH.HH 0, 24.72, 17.75
ASP178OD1-TYR169@HH 35.55, 0, 0	ASP178@OD2-ARG$^+$164@NE.HE 36.29, 0, 0	ASP178@OD1-TYR128@OH.HH 0, 12.25, 6.50
ASP178OD2-TYR169@HH 40.47, 0, 0	ASP178@OD2-ARG$^+$164@NH2.HH21 30.03, 23.94, 20.27	ASP178@OD2-TYR128@OH.HH 0, 12.47, 5.90
	ASP178@OD1-TYR169@OH.HH 32.27, 25.65, 57.75	GLU221@OE1-SER167@OG.HG 11.70, 0, 0
	ASP178@OD2-TYR169@OH.HH 0, 11.96, 30.44	GLU221@OE2-SER167@OG.HG 10.38, 0, 0
	GLU221@OE1-TYR163@OH.HH 23.40, 0, 26.15	LEU138@O-TYR150@OH.HH 0, 10.75, 0
	GLU221@OE2-TYR163@OH.HH 24.55, 14.65, 25.87	GLY126@O-ARG$^+$164@NH2.HH21 0, 0, 15.48
	PRO158@O-ARG$^+$136@NE.HE 0, 10.81, 0	GLY127@O-ARG$^+$164@NE.HE 0, 0, 14.48
	ASP178@OD1-TYR128@OH.HH 6.19, 35.51, 50.43	GLY131@O-GLN160@NE2.HE21 0, 0, 13.70
	ASP178@OD2-TYR128@OH.HH 5.35, 22.53, 38.97	GLU146@OE1-ARG$^+$208@NE.HE 0, 0, 11.57
		GLU146@OE1-ARG$^+$208@NH2.HH21 5.88, 5.28, 11.72
		GLU146@OE2-ARG$^+$208@NH2.HH21 5.18, 0, 13.53

Table 4. SBs (with an occupancy rate > 5%) of the WT during the three sets of 30 ns MD simulations under a neutral pH environment at 300 K, 350 K and 450 K (from left to right in turns: 300 K seed1–seed3, 350 K seed1–seed3, 450 K seed1–seed3).

SBs at 300 K under Neutral pH Environment	SBs at 350 K under Neutral pH Environment	SBs at 450 K under Neutral pH Environment
ASP147@CG-ARG$^+$148@CA.CZ 100, 100, 100	ASP147@CG-ARG$^+$148@CA.CZ 100, 100, 100	ASP147@CG-ARG$^+$148@CA.CZ 100, 100, 100
GLU211@CD-ARG$^+$208@CA.CZ 99.99, 98.53, 99.88	GLU211@CD-ARG$^+$208@CA.CZ 99.75, 99.49, 99.19	GLU211@CD-ARG$^+$208@CA.CZ 98.50, 99.32, 97.43
GLU207@CD-LYS$^+$204@CA.NZ 99.70, 92.81, 99.90	GLU207@CD-LYS$^+$204@CA.NZ 99.58, 95.18, 94.64	GLU207@CD-LYS$^+$204@CA.NZ 81.43, 95.43, 95.37
GLU221@CD-LYS$^+$220@CA.NZ 99.18, 95.05, 99.53	GLU221@CD-LYS$^+$220@CA.NZ 95.19, 75.51, 95.72	GLU152@CD-ARG$^+$148@CA.CZ 79.35, 37.07, 30.50
GLU207@CD-ARG$^+$208@CA.CZ 97.93, 89.95, 90.66	GLU223@CD-LYS$^+$220@CA.NZ 84.79, 88.04, 89.61	GLU223@CD-LYS$^+$220@CA.NZ 52.90, 84.60, 85.40
GLU223@CD-LYS$^+$220@CA.NZ 83.49, 86.61, 84.31	HID177@CG-LYS$^+$173@CA.NZ 89.28, 68.55, 83.69	GLU207@CD-ARG$^+$208@CA.CZ 78.65, 77.78, 71.73
HID177@CG-LYS$^+$173@CA.NZ 76.03, 54.27, 59.23	HID177@NE2-LYS$^+$173@CA.NZ 84.88, 59.56, 79.02	GLU152@CD-ARG$^+$151@CA.CZ 64.87, 41.73, 48.42
ASP178@CG-ARG$^+$164@CA.CZ 8.54, 80.97, 72.61	GLU207@CD-ARG$^+$208@CA.CZ 82.31, 75.41, 70.49	GLU221@CD-LYS$^+$220@CA.NZ 59.77, 67.45, 71.52
ASP144@CG-ARG$^+$148@CA.CZ 56.94, 63.26, 81.40	ASP144@CG-ARG$^+$148@CA.CZ 69.22, 66.07, 69.63	HID177@CG-LYS$^+$173@CA.NZ 35.13, 61.08, 61.32
HID187@NE2-ARG$^+$156@CA.CZ 75.33, 79.47, 78.88	GLU196@CD-LYS$^+$194@CA.NZ 80.79, 46.75, 13.83	HID177@NE2-LYS$^+$173@CA.NZ 24.10, 50.62, 48.95
HID177@NE2-LYS$^+$173@CA.NZ 73.13, 44.92, 48.37	GLU152@CD-ARG$^+$148@CA.CZ 19.88, 51.91, 50.99	ASP147@CG-HID$^+$140@ND1.HD1 57.98, 56.63, 71.32
ASP147@CG-HID$^+$140@ND1.HD1 32.85, 59.40, 5.03	HID187@NE2-ARG$^+$156@CA.CZ 8.05, 50.02, 68.03	ASP147@CG-ARG$^+$151@CA.CZ 53.13, 57.55, 52.87
GLU152@CD-ARG$^+$148@CA.CZ 41.30, 57.81, 22.23	ASP147@CG-HID$^+$140@ND1.HD1 66.73, 14.95, 50.97	ASP144@CG-ARG$^+$148@CA.CZ 46.73, 40.42, 42.32
GLU152@CD-ARG$^+$151@CA.CZ 40.62, 24.43, 46.85	ASP147@CG-ARG$^+$151@CA.CZ 40.29, 51.06, 19.25	GLU168@CD-ARG$^+$164@CA.CZ 18.28, 42.77, 9.27
ASP147@CG-ARG$^+$151@CA.CZ 24.14, 6.27, 36.33	GLU168@CD-ARG$^+$164@CA.CZ 38.75, 33.56, 57.47	GLU146@CD-ARG$^+$208@CA.CZ 5.67, 19.18, 13.50
ASP178@CG-HID$^+$177@ND1.HD1 5.60, 14.60, 21.83	GLU152@CD-ARG$^+$151@CA.CZ 65.20, 42.93, 42.81	ASP178@CG-HID$^+$177@ND1.HD1 16.07, 17.85, 19.48
GLU211@CD-HID$^+$177@ND1.HD1 20.18, 8.37, 12.57	GLU196@CD-ARG$^+$156@CA.CZ 17.17, 41.71, 43.47	GLU211@CD-HID$^+$177@ND1.HD1 16.42, 16.27, 12.23
GLU196@CD-LYS$^+$194@CA.NZ 0, 63.33, 0	GLU211@CD-HID$^+$177@ND1.HD1 27.48, 15.45, 17.77	HID187@CG-LYS$^+$185@CA.NZ 38.85, 5.92, 0
GLU168@CD-ARG$^+$164@CA.CZ 52.00, 0, 8.60	ASP178@CG-HID$^+$177@ND1.HD1 10.42, 14.12, 8.83	ASP178@CG-ARG$^+$164@CA.CZ 0, 22.00, 38.58
GLU196@CD-ARG$^+$156@CA.CZ 0, 9.63, 0	ASP178@CG-ARG$^+$164@CA.CZ 10.45, 33.61, 0	GLU152@CD-ARG$^+$156@CA.CZ 34.87, 0, 0
ASP202@CG-ARG$^+$156@CA.CZ 0, 6.53, 0	GLU223@CD-ARG$^+$228@CA.CZ 0, 0, 10.11	HID187@NE2-LYS$^+$185@CA.NZ 25.88, 0, 0
	HID187@CG-ARG$^+$156@CA.CZ 0, 0, 7.57	GLU196@CD-LYS$^+$194@CA.NZ 0, 24.88, 14.97
	ASP202@CG-ARG$^+$156@CA.CZ 0, 0, 6.69	HID187@NE2-ARG$^+$156@CA.CZ 0, 15.08, 24.72
	ASP144@CG-HID$^+$140@ND1.HD1 7.40, 0, 0	GLU146@CD-HID$^+$140@ND1.HD1 24.42, 0, 16.37
		ASP144@CG-HID$^+$140@ND1.HD1 0, 5.23, 19.77
		GLU196@CD-ARG$^+$156@CA.CZ 0, 16.48, 16.42
		HID140@NE2-ARG$^+$136@CA.CZ 14.30, 0, 0
		ASP202@CG-LYS$^+$194@CA.NZ 0, 12.78, 14.15
		GLU168@CD-ARG$^+$228@CA.CZ 9.57, 0, 0
		ASP202@CG-ARG$^+$156@CA.CZ 9.35, 0, 0

Table 4. *Cont.*

SBs at 300 K under Neutral pH Environment	SBs at 350 K under Neutral pH Environment	SBs at 450 K under Neutral pH Environment
		GLU200@CD-HID$^+$187@ND1.HD1 8.30, 0, 0
		GLU146@CD-LYS$^+$204@CA.NZ 0, 5.88, 5.47
		HID140@NE2-ARG$^+$208@CA.CZ 0, 0, 11.40
		HID140@CG-ARG$^+$136@CA.CZ 7.42, 0, 0
		GLU200@CD-LYS$^+$194@CA.NZ 0, 0, 10.70
		GLU221@CD-ARG$^+$228@CA.CZ 7.33, 0, 0
		GLU207@CD-HID$^+$177@ND1.HD1 6.42, 5.13, 0

Table 5. HYDs (with an occupancy rate of 100%) of the WT at 300 K, 350 K and 450 K during 30 ns MD simulations whether under low or neutral pH environments.

Under Low-pH Environment	Under Neutral pH Environment	Position in the PrP Structure
PHE225@CB-ALA224@CA.C	PHE225@CB-ALA224@CA.C	Within α3
ALA224@CB-PHE225@CA.C	ALA224@CB-PHE225@CA.C	Within α3
VAL210@CB-VAL209@CA.C	VAL210@CB-VAL209@CA.C	Within α3
VAL209@CB-VAL210@CA.C	VAL209@CB-VAL210@CA.C	Within α3
VAL209@CB-MET206@CA.C	VAL209@CB-MET206@CA.C	Within α3
MET206@CB-ILE205@CA.C	MET206@CB-ILE205@CA.C	Within α3
ILE205@CB-MET206@CA.C	ILE205@CB-MET206@CA.C	Within α3
VAL176@CB-PHE175@CA.C	VAL176@CB-PHE175@CA.C	Within α2
PHE175@CB-VAL176@CA.C	PHE175@CB-VAL176@CA.C	Within α2
VAL166@CB-PRO165@CA.C	VAL166@CB-PRO165@CA.C	Within β2-3_{10}H2-loop
PRO165@CB-VAL166@CA.C	PRO165@CB-VAL166@CA.C	Within β2-3_{10}H2-loop
ILE139@CB-LEU138@CA.C	ILE139@CB-LEU138@CA.C	Within β1-α1-loop
LEU138@CB-ILE139@CA.C	LEU138@CB-ILE139@CA.C	Within β1-α1-loop
LEU138@CB-PRO137@CA.C	LEU138@CB-PRO137@CA.C	Within β1-α1-loop
PRO137@CB-LEU138@CA.C	PRO137@CB-LEU138@CA.C	Within β1-α1-loop
MET134@CB-ALA133@CA.C	MET134@CB-ALA133@CA.C	Linking β1 and β1-α1-loop
ALA133@CB-MET134@CA.C	ALA133@CB-MET134@CA.C	Linking β1 and β1-α1-loop
LEU130@CB-MET129@CA.C	LEU130@CB-MET129@CA.C	Within β1
MET129@CB-LEU130@CA.C	MET129@CB-LEU130@CA.C	Within β1
VAL122@CB-VAL121@CA.C	VAL122@CB-VAL121@CA.C	Within N-terminal
VAL121@CB-VAL122@CA.C	VAL121@CB-VAL122@CA.C	Within N-terminal
MET213@CB-VAL210@CA.C 99.98, 100, 99.98	MET213@CB-VAL210@CA.C 99.97, 100, 100	Within α3
MET206@CB-VAL203@CA.C 95.20, 100, 99.93	MET206@CB-VAL203@CA.C 100, 99.90, 100	Within α3

Table 6. Some special HYDs (with an occupancy rate of almost 100%) of the WT at 300 K and 350 K during 30 ns MD simulations under a neutral pH environment.

300 K—Under Neutral pH Environment	350 K—Under Neutral pH Environment		Position in the PrP Structure
VAL210@CB-VAL180@CA.C	VAL210@CB-VAL180@CA.C	100% exist at 300 K—low pH	Linking α3 and α2
MET213@CB-VAL161@CA.C	MET213@CB-VAL161@CA.C		Linking α3 and β2
VAL161@CB-MET213@CA.C	VAL161@CB-MET213@CA.C		Linking β2 and α3
VAL176@CB-ILE215@CA.C			Linking α2 and α3

Table 2 shows us the following when compared with a neutral pH environment: (i) at 300 K, H α-helices become less frequent and E β-strands become more frequent under a

low-pH environment; (ii) at 350, the number of K G 3_{10}-helices decreases, for seed3 the number of I π-helices decreases, for seed2 and seed3 the number of H α-helices decreases, and for seed2 the number of E β-strands decreases under a low-pH environment; and (iii) at 450 K, the number of B β-bridges increases, for seed1 the number of G 3_{10}-helices decreases, for seed3 the number of I π-helices decreases, for seed2 and seed3 the number of H α-helices decreases, and for seed1 and seed2 the number of E β-strands increases under a low-pH environment. From Table 2, we can see PrP^C is predominant in α-helices—being at least 38.34% α-helix. Under a neutral pH environment, the percentages of α-helix become lower and lower as the temperatures go up from 300 K to 350 K and to 450 K; however, under a low-pH environment this rule is not obeyed for seed2 and seed3 from 300 K to 350 K. PrP^C has a β-sheet structure of about 3%, and at 300 K the change from a neutral pH environment to a low-pH environment increases the percentage of β-sheet (Table 2).

In Figure S1, we notice that at 300 K (i) under a neutral pH environment, for seed2 during 0–11.8 ns the α2 C-terminal segment aa 189–195 is in a turn structure, and for seed1 and seed3 the α3 N-terminal segment aa 200–201 is also in a turn structure; and (ii) under a low-pH environment, for seed2 during the 0–9.4 ns the segment aa 160–161 has an extension of β1 sheet structure and for seed3 the α3 C-terminal segment 220–226 is in a turn structure.

In Figure S2, we notice that at 350 K under a neutral pH environment for seed1 (i) the β1 E β-strand structure extends to the segment aa 120–130 and (ii) the α1 H α-helix structure unfolds in the segment aa 152–157 during 13–30 ns.

In Figure S3, we notice that at 450 K (i) under a neutral pH environment, for seed1 the E β-sheet's two β-strands are broken, for seed2 the β-sheet structure becomes a β-bridge structure during 9–17.4 ns and for all seeds the N- and C-terminals of α1, α2 and α3 unfold; and (ii) under a low-pH environment, the β-sheet is broken for seed1, becomes a β-bridge for seed2 and is broken for seed3 from 18 ns, and for seed3 α1 unfolds from 20.6 ns, α2 is unfolding from 26.6 ns (Figure 4)—we should also notice the RMSD values steadily go up under a low-pH environment at 450 K (Figure 4.9a of [18]).

Generally, for WT, the above secondary structures results (shown in Table 2 and Figures S1–S3), in combination with the RMSD (root mean square deviation), radius of gyration, RMSF (RMS fluctuation) and B-factor results in Section 4.1 of [18], show us that at 450 K under a low-pH environment (compared with under a neutral pH environment) α-helices start to unfold and the number of β-strands/bridges increases.

Let us review the analyses on the HBs, SBs and HYDs of the WT. Under a low-pH environment at MD-production constant temperatures of 300 K, 350 K and 450 K, all the HBs in Table 3 were removed. Under a neutral pH environment, at temperature levels of 300 K, 350 K and 450 K, the HBs ASP202-ARG+156/TYR157/TYR149 and ASP178-ARG+164/TYR128/TYR169 always exist (Table 3). Here, we should note that there exists an HB ASP178@O-TYR128@OH.HH 11.81 for seed1 at 350 K under a low-pH environment. In addition, in Table 3 the following HBs also contribute to the structural stability of the WT under a neutral pH environment: GLU146-LYS+204 and GLN172-GLN219 at 300 K; GLU196-ARG+156 and GLU221-TYR163 and PRO158-ARG+136 at 350 K; and GLU196-GLY119/SER120 and GLU221-SER167 and LEU138-TYR150 and GLY126/GLY127-ARG+164 and GLY131-GLN160 and GLU146-ARG+208 at 450 K.

Table 4 lists all the SBs (with occupancy rates > 5%) of the WT under a neutral pH environment at 30 ns MD-production constant temperatures of 300 K, 350 K and 450 K. All the SBs of 300 K (ASP144-ARG^+148, ASP147-HID^+140/ARG^+148/ARG^+151, HID177-LYS^+173, ASP178-ARG^+164, HID187-ARG^+156, GLU152-ARG^+148/ARG^+151, GLU168-ARG^+164, GLU196-ARG^+156/LYS^+194, ASP202-ARG^+156, GLU207-LYS^+204/ARG^+208, GLU211-HID^+177/ARG^+208/LYS^+220, GLU223-LYS^+220) still exist at 350 K and 450 K. In addition, at 350 K there are the additional SBs GLU223@CD-ARG^+228@CA.CZ and HID187@CG-ARG^+156@CA.CZ and ASP144@CG-HID^+140@ND1.HD1; and at 450 K there are the additional SBs GLU146@CD-ARG^+208@CA.CZ, HID187@CG-LYS^+185@CA.NZ, GLU152@CD-ARG^+156@CA.CZ, HID187@NE2-LYS^+185@CA.NZ, GLU146@CD-HID^+140@ND1.HD1,

ASP144@CG-HID$^+$140@ND1.HD1, HID140@NE2-ARG$^+$136@CA.CZ, ASP202@CG-LYS$^+$194 @CA.NZ, GLU168@CD-ARG$^+$228@CA.CZ, GLU200@CD-HID$^+$187@ND1.HD1, GLU146@C D-LYS$^+$204@CA.NZ, HID140@NE2-ARG$^+$208@CA.CZ, HID140@CG-ARG$^+$136@CA.CZ, GLU200@CD-LYS$^+$194@CA.NZ, GLU221@CD-ARG$^+$228@CA.CZ and GLU207@CD-HID$^+$1 77@ND1.HD1. From Tables 3 and 4, we may observe that the polar contacts ASP178-ARG$^+$164, ASP202-ARG$^+$156 (weaker), GLU196-ARG$^+$156, GLU146-ARG$^+$208 (strong only at 450 K) contribute to the structural stability of the WT during the MD simulations. The positions of the special SBs (HID187-ARG$^+$156 (linking α2 and 310H1), GLU211-HID$^+$177 (linking α3 and α2)), the special polar contacts (ASP178-ARG$^+$164 (linking α2 and β2-3_{10}H2-loop), ASP202-ARG$^+$156 (linking α3 and 3_{10}H1), GLU196-ARG$^+$156 (linking α2-α3-loop and 3_{10}H1), GLU146-ARG$^+$208 (linking α1 and α3)) and the SBs (GLU223-LYS$^+$220, GLU207-LYS$^+$204/ARG$^+$208, GLU211-ARG$^+$208/LYS$^+$220, GLU223-LYS$^+$220 within α3, HID177-LYS$^+$173 within α2, ASP144-ARG$^+$148, ASP147-ARG$^+$148/ARG$^+$151 within α1, GLU196-LYS$^+$194 within the α2-α3-loop, GLU152-ARG$^+$148/ARG$^+$151 linking the α1-3_{10}H1-loop with α1, GLU168-ARG$^+$164 linking the β2-3_{10}H2-loop and 3_{10}H2 and ASP147-HID$^+$140 linking α1 and the β1-α1-loop) should be noticed.

Table 5 lists the basic HYDs (with an occupancy rate of 100%) maintained all the time under low or neutral pH environments at 300 K or 350 K or 450 K—all these basic HYDs are always contributing to the structural stability of the WT.

For HYDs, we also find some special and important HYDs listed in Table 6, which disappeared under a low-pH environment (except for the HYD VAL210@CB-VAL180@CA.C at 300 K under a low-pH environment) and completely disappeared at the higher temperature of 450 K. From Table 6, we know that the HYD VAL176@CB-ILE215@CA.C contributes to the stability at 300 K under a neutral pH environment, the HYD VAL210@CB-VAL180@CA.C contributes to the stability at 300 K under a low-pH environment, and the HYDs VAL210@CB-VAL180@CA.C, MET213@CB-VAL161@CA.C and VAL161@CB-MET213@CA.C not only contribute to the stability under a neutral pH environment at 300 K but also at 350 K. In total, 100% of these HYDs disappeared at 450 K. Generally, we can see that a low-pH environment or/and higher temperature will make the protein structural stability weaker.

In [12], we were told that the NMR structure of horse PrP^C at 25 degrees C contains a well-structured and highly structurally ordered β2-α2-loop; with α3, this loop forms a binding site for a chaperone 'protein X,' and within this loop the single amino acid S167 is unique to the PrP sequences of equine species. S167 was reported to be a protective residue for horse PrP^C. Our secondary structure WT MD studies show us two performances: (i) for the WT, the N-terminal half of α1 is not stable and the β2-α2-loop has less variations than other loops; but (ii) from the optimised structures for the mutant (compared with the WT), it is unstable in the regions of α2 and α3 (especially at both terminals of α2) and in the binding site for 'protein X.' Detailed HBs, SBs and HYDs bioinformatics to explain the reasons for the performances were presented from the analyses of our WT MD results.

In summary, the author sets out to investigate the molecular differences between the wild type (WT) horse prion protein and its S167D mutant which increases the susceptibility to prion diseases, using molecular dynamics (MD). The author then claims that, based on the S167D mutation resulting in some lost HBs and SBs in α2 and α3 and some lost π-cations, we may see the molecular structure of the mutant (compared with the WT) is unstable especially in the regions of α2 and α3 (especially at both terminals of α2) compared to the WT. While purporting to elucidate the structural differences between the WT and mutant horse prion protein, this article reports no results from the MD simulations for the mutant, because the experimental structure of the mutant is not currently available. Various secondary structural statistics for the mutant simulations at different temperatures and pH conditions, and the changes in the H-bond network caused by the mutation with MD simulations, should be presented. Although the molecular mechanism of neurodegenerative diseases in the cases involving prion proteins is still unclear, it is hypothesized to involve the growth of amyloid fibrils via the process of oligomerization (hence the higher beta-sheet

population). Here, we used a well-folded helical protein monomer as the initial structure and ran MD simulations on a timescale (30 ns) much shorter than the one we required to observe significant protein conformational change; it is therefore still unclear how probative these simulations are of the biological process we are trying our best to model. However, the secondary structure time-series plots (Figures S1–S3) are highly effective, providing us many representative structural clusters/snapshots to show us that for the WT under low-pH conditions it is much more unstable than under neutral pH conditions, though a longer MD timescale is still needed to understand further. The simulations are very short (30 ns) to verify structural change. The simulation time should be increased and the conformational changes should be noted as soon as the computing resources are available from NCI Australia.

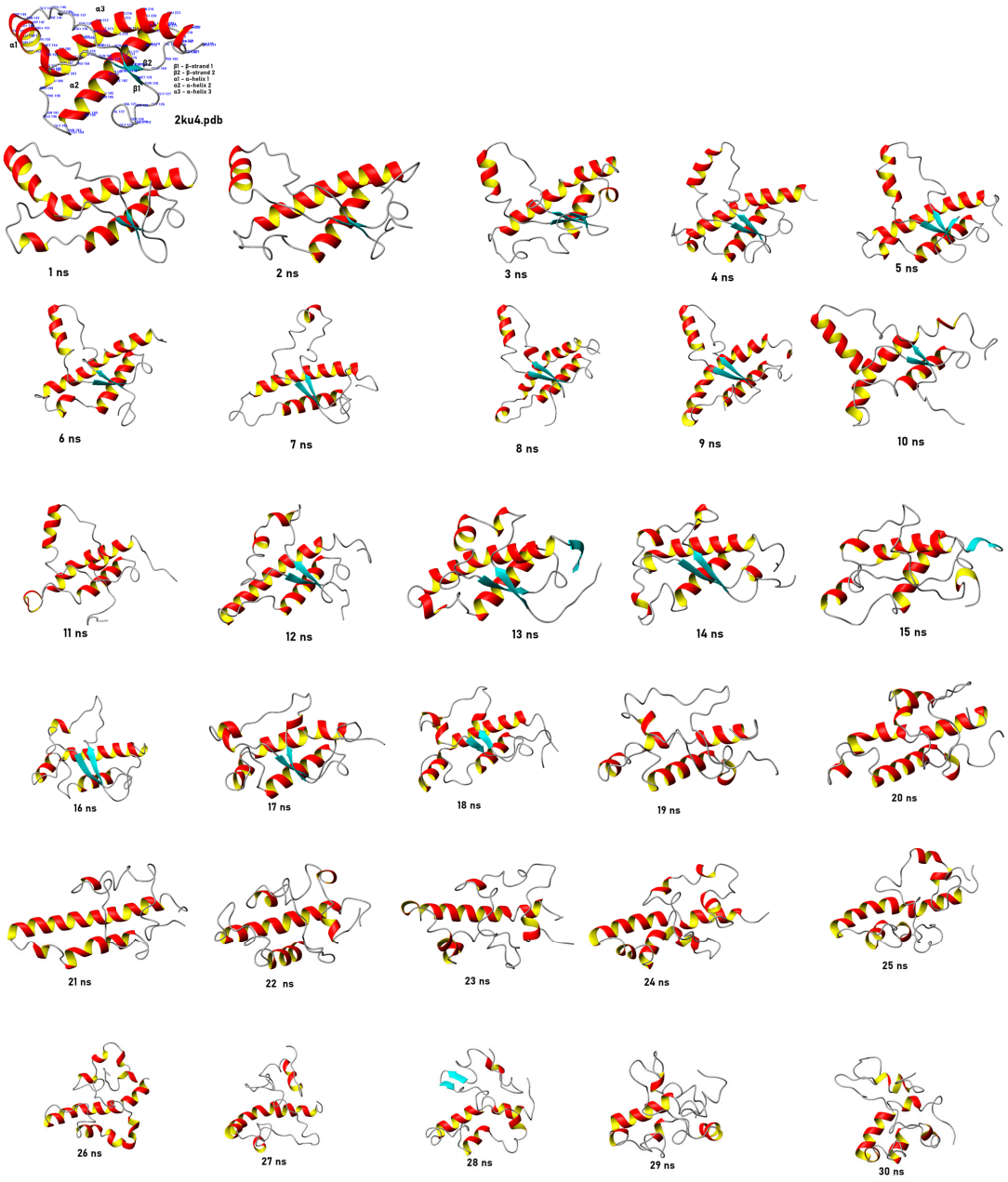

Figure 4. The 30 snapshots of three-dimensional molecular structures of the horse PrP wild type for the S3f—30 ns MD at 450 K low-pH seed3: the β-sheet is broken from 18 ns, α1 unfolds from 20.6 ns and α2 unfolds from 26.6 ns. The first graph is the NMR structure of 2ku4.pdb for comparisons with the 30 snapshots.

For the horse PrP S167D mutant, there are currently no literature data, and no experimental structure has yet been produced. But for the horse PrP^C WT, in Sections 5.2 and 5.3 of [19] and Section 4.1 of [18] there are rich bibliographic reviews and comparisons with rabbit PrP^C and dog PrP^C, though updates are needed.

This article is not to study the interactions of PrP with the solvent and the ions, and there is no ligand in this study for PrP binding so that we did not include the interaction energies with the solvent (like [20] for example) nor did we calculate the energies using methods such as MM/PBSA. However, the free energy calculations are a research direction for this article to investigate the effects/contributions of ions such as Cu^{2+} and of solvents such as water. This should be highlighted as a future research direction for the author.

4. Conclusions

In summary, the molecular structure of the mutant (compared with the WT) is unstable especially in the regions of α2 and α3 (especially at both terminals of α2), and S167 is a critical contribution to WT horse PrP^C structure stability. The S167D mutation resulted in the WT losing (i) its SBs such as ASP147-ARG148 (in α1), ASP147-ARG151 (in α1), ASP178-HIS177 (in α2), ASP202-ARG156 (linking α3-3_{10}H1), GLU152-ARG151 (linking α1-3_{10}H1-loop-α1), GLU168-ARG164 (linking 3_{10}H2-β2-3_{10}H2-loop) and GLU211-ARG208 (in α3); (ii) an important polar contact ASP202-ARG^+156; (iii) two π-cations, PHE141-ARG208.$NH2^+$ (linking β1-α1-loop-α3) and HIS177-LYS173.NZ^+ (in α2); and (iv) one important HB, GLU221-SER167; and it redistributed the negative charges on the surface around the β2-α2-loop region so that the well-defined and highly ordered β2-α2-loop structure of WT horse PrP^C has more variations in the mutant. Our WT MD results in this article have confirmed that the single amino acid differences at position 167 might influence the overall protein structures of the WT.

Supplementary Materials: The following supporting information can be downloaded at https://www.mdpi.com/article/10.3390/zoonoticdis4030017/s1, Figures S1–S3 are the MD secondary structures for the WT at 300 K, 350 K and 450 K, respectively, where the MDs are the 30 ns MD simulations (seed1, seed2, seed3) in neutral and low-pH environments.

Funding: This research (with Project No. pb04 at Federation University Australia and under NCI) was undertaken with the assistance of resources and services from the National Computational Infrastructure (NCI), which is supported by the Australian Government.

Institutional Review Board Statement: Not applicable.

Informed Consent Statement: Not applicable.

Data Availability Statement: The original contributions presented in the study are included in the article/Supplementary Material, further inquiries can be directed to the corresponding author.

Conflicts of Interest: The authors declare no conflicts of interest.

Abbreviation

SBs	salt bridges
HBs	hydrogen bonds
HYDs	hydrophobic interactions
vdWs	van der Waals
aa	amino acid (or residue)
S-S	disulfide bond

References

1. Vorberg, I.; Martin, H.G.; Eberhard, P.; Suzette, A.P. Multiple amino acid residues within the rabbit prion protein inhibit formation of its abnormal isoform. *J. Virol.* **2003**, *77*, 2003–2009. [CrossRef] [PubMed]
2. Wen, Y.; Li, J.; Xiong, M.Q.; Peng, Y.; Yao, W.M.; Hong, J.; Lin, D.H. Solution structure and dynamics of the I214V mutant of the rabbit prion protein. *PLoS ONE* **2010**, *5*, e13273. [CrossRef] [PubMed]

3. Wen, Y.; Li, J.; Yao, W.M.; Xiong, M.Q.; Hong, J.; Peng, Y.; Xiao, G.F.; Lin, D.H. Unique structural characteristics of the rabbit prion protein. *J. Biol. Chem.* **2010**, *285*, 31682–31693. [CrossRef] [PubMed]
4. Khan, M.Q.; Sweeting, B.; Mulligan, V.K.; Arslan, P.E.; Cashman, N.R.; Pai, E.F.; Chakrabartty, A. Prion disease susceptibility is affected by β-structure folding propensity and local side-chain interactions in PrP. *Proc. Natl. Acad. Sci. USA* **2010**, *107*, 19808–19813. [CrossRef] [PubMed]
5. Sweeting, B.; Brown, E.; Khan, M.Q.; Chakrabartty, A.; Pai, E.F. N-terminal helix-cap in α-helix 2 modulates β-state misfolding in rabbit and hamster prion proteins. *PLoS ONE* **2013**, *8*, e63047. [CrossRef] [PubMed]
6. Polymenidoua, M.; Trusheimb, H.; Stallmacha, L.; Moosa, R.; Julius, J.A.; Mielea, G.; Lenzbauerb, C.; Aguzzia, A. Canine MDCK cell lines are refractory to infection with human and mouse prions. *Vaccine* **2008**, *26*, 2601–2614. [CrossRef] [PubMed]
7. Hasegawa, K.; Mohri, S.; Yokoyama, T. Comparison of the local structural stabilities of mammalian prion protein (PrP) by fragment molecular orbital calculations. *Prion* **2013**, *7*, 185–191. [CrossRef] [PubMed]
8. Sanchez-Garcia, J.; Jensen, K.; Zhang, Y.; Rincon-Limas, D.E.; Fernandez-Funez, P. A single amino acid (Asp159) from the dog prion protein suppresses the toxicity of the mouse prion protein in Drosophila. *Neurobiol. Dis.* **2016**, *95*, 204–209. [CrossRef] [PubMed]
9. Fernández-Borges, N.; Parra, B.; Vidal, E.; Eraña, H.; Sánchez-Martín, M.A.; de Castro, J.; Elezgarai, S.R.; Pumarola, M.; Mayoral, T.; Castilla, J. Unraveling the key to the resistance of canids to prion diseases. *PLoS Pathog.* **2017**, *13*, e1006716. [CrossRef] [PubMed]
10. Lysek, D.A.; Schorn, C.; Nivon, L.G.; Esteve-Moya, V.; Christen, B.; Calzolai, L.; von Schroetter, C.; Fiorito, F.; Herrmann, T.; Guntert, P. Prion protein NMR structures of cats, dogs, pigs, and sheep. *Proc. Natl. Acad. Sci. USA* **2005**, *102*, 640–645. [CrossRef] [PubMed]
11. Zhang, J.P. Molecular dynamics studies of dog prion protein wild-type and its D159N mutant. *J. Biomol. Struct. Dyn.* **2021**, *39*, 4234–4242. [CrossRef] [PubMed]
12. Perez, D.R.; Damberger, F.F.; Wuthrich, K. Horse prion protein NMR structure and comparisons with related variants of the mouse prion protein. *J. Mol. Biol.* **2010**, *400*, 121–128. [CrossRef] [PubMed]
13. Zhang, J.P. The structural stability of wild-type horse prion protein. *J. Biomol. Struct. Dyn.* **2011**, *29*, 369–377. [CrossRef]
14. Fernández-Funez, P. The Prion Protein Zoo: Identification of Protective Residues from Prion-Resistant Animals. Available online: http://www.cajal.csic.es/actividades2017/2017-10-30-PedroFernandezSketch.pdf (accessed on 29 September 2021).
15. Myers, R.R.; Sanchez-Garcia, J.; Leving, D.C.; Fernandez-Funez, P. New Drosophila models to uncover the intrinsic and extrinsic factors mediating the toxicity of the human prion protein. *Dis. Model. Mech.* **2022**, *15*, dmm049184. [CrossRef] [PubMed]
16. Myers, R.; Cembran, A.; Fernandez-Funez, P. Insight from animals resistant to prion diseases: Deciphering the genotype—Morphotype–phenotype code for the prion protein. *Front. Cell Neurosci.* **2020**, *14*, 254. [CrossRef]
17. Zhang, J.P. *Optimization-Based Molecular Dynamics Studies of SARS-CoV-2 Molecular Structures—Research on COVID-19*; Springer: Cham, Switzerland, 2023.
18. Zhang, J.P. *Structural Dynamics Analyses of Prion Protein Structures—The Resistance to Prion Diseases Down Under*; Springer: Singapore, 2018; pp. 5–12.
19. Zhang, J.P. *Molecular Structures and Structural Dynamics of Prion Proteins and Prions—Mechanism Underlying the Resistance to Prion Diseases*; Springer: Dordrecht, The Netherlands, 2015.
20. Zazeri, G.; Povinelli, A.P.R.; Pavan, N.M.; Jones, A.M.; Ximenes, V.F. Solvent-induced lag phase during the formation of lysozyme amyloid fibrils triggered by sodium dodecyl sulfate: Biophysical experimental and in silico study of solvent effects. *Molecules* **2023**, *28*, 6891. [CrossRef]